Neutrino electromagnetic properties and the weak mixing angle at the LHC Forward Physics Facility

Roshan Mammen Abraham[1,*] Saeid Foroughi-Abari[2,†] Felix Kling[3,‡] and Yu-Dai Tsai[4,§]

[1]*Department of Physics, Oklahoma State University, Stillwater, Oklahoma, 74078, USA*
[2]*Department of Physics and Astronomy, University of Victoria, Victoria, British Columbia V8P 5C2, Canada*
[3]*Deutsches Elektronen-Synchrotron DESY, Germany*
[4]*Department of Physics and Astronomy, University of California, Irvine, California 92697-4575, USA*

The LHC produces an intense beam of highly energetic neutrinos of all three flavors in the forward direction, and the Forward Physics Facility (FPF) has been proposed to house a suite of experiments taking advantage of this opportunity. In this study, we investigate the FPF's potential to probe the neutrino electromagnetic properties, including neutrino millicharge, magnetic moment, and charge radius. We find that, due to the large flux of tau neutrinos at the LHC, the FPF detectors will be able to provide more sensitive constraints on the tau neutrino magnetic moment and millicharge than previous measurements at DONUT, by searching for excess in low recoil energy electron scattering events. We also find that, by precisely measuring the rate of neutral current deep inelastic scattering events, the FPF detectors have the potential to obtain the strongest experimental bounds on the neutrino charge radius for the electron neutrino, and one of the leading bounds for the muon neutrino flavor. The same signature could also be used to measure the weak mixing angle, and we estimate that $\sin^2\theta_W$ could be measured to about 3% precision at a scale $Q \sim 10$ GeV, shedding new light on the longstanding NuTeV anomaly.

I. INTRODUCTION

Neutrino properties are crucial to understanding our Universe and have been prime targets of particle physics experiments. The electromagnetic (EM) properties of neutrinos, in particular, can be tested in existing and future experiments. These measurements include the mass-dimension 4 neutrino millicharge, the mass-dimension 5 neutrino dipole moments, and the mass-dimension 6 neutrino charge radius. These properties can, for example, be used to determine whether neutrinos have a Dirac or Majorana nature [1,2] and to probe new physics beyond the Standard Model (SM) [3]. These neutrino properties could be linked to intriguing experimental anomalies, including the NuTeV anomaly [4] and the Xenon 1T excess [5] (although the latter was determined most likely to be from an SM background [6]). Large neutrino dipole moments, for

example, can also affect the mass gap of black holes [7,8]. Interesting models were proposed to generate neutrino EM couplings much larger than the SM predictions [9–14] and to connect the anomalies to the neutrino properties [15]. Currently, the SM predictions of these properties are several orders of magnitude smaller than the present upper bounds, obtained from reactor neutrinos [16,17], accelerator neutrinos [18–20], and solar neutrinos [6,21–25], to name a few. For a connection between neutrino electromagnetic properties and *CP* phases, see Ref. [26].

The LHC provides one of the most exciting opportunities in studying high-energy neutrinos and tau neutrinos, given its high center-of-mass energy. The forward region at the LHC, in particular, provides a large flux of neutrinos coming from meson decays [27]. The Forward Physics Facility (FPF) [28] at the LHC is ideally placed on studying these TeV energy neutrinos. Previously, interesting signatures from the neutrino dipole portal [29,30], were studied at FPF [31] and FASER [32], but a proper analysis of the future capability of FPF on neutrino EM properties are sorely lacking at this moment.

In this letter, we utilize the FPF to study interesting properties of neutrinos: the neutrino millicharge, magnetic moment, and charge radius. By looking at low recoil energy electron scattering and neutral current deep inelastic scattering (DIS) events, we show that we can reach competitive sensitivity for these properties. Most excitingly, we can set

*Contact author: rmammen@okstate.edu
†Contact author: saeidf@uvic.ca
‡Contact author: felix.kling@desy.de
§Contact author: yudait1@uci.edu, yt444@cornell.edu

the world's leading limit on neutrino charge radius for the electron neutrino, while for the muon neutrino, we come within a factor of a few from the SM prediction. For the tau neutrino, FPF's limits on the magnetic moment are an order of magnitude better than the DONUT results [19] and bounds on millicharge and charge radius constitute some of the few existing measurements for the tau neutrino.

The neutrino interactions with the target material, investigated in this study, also depend sensitively on electroweak parameters. In this context, the precise measurement of the neutral current neutrino DIS rate can also be translated to a precise measurement of the weak mixing angle. This would allow one to test the anomalous result obtained by NuTeV [4].

The paper is organized as follows. We briefly review neutrino EM properties in Sec. II and introduce the detectors under consideration at the FPF in Sec. III. In Sec. IV, we discuss our signal characteristics. We present our results on the neutrino EM properties in Sec. V and discuss the measurement of the weak mixing angle in Sec. VI. We conclude in Sec. VII.

II. NEUTRINO EM PROPERTIES

The electric charge of neutrinos is zero in the SM. However, electromagnetic properties can arise at the quantum loop level (or via BSM physics) allowing electromagnetic interactions of neutrinos with photons and charged particles. Considering neutrinos as massive fermions, the electromagnetic properties of neutrinos in the one-photon approximation can be assembled in the matrix element of the neutrino effective electromagnetic current [33,34] as

$$\langle \nu_f(p_f)|j^\mu_{\nu,\mathrm{EM}}|\nu_i(p_i)\rangle = \bar{u}_f(p_f)\Lambda^\mu_{fi}(q)u_i(p_i), \quad (1)$$

where q is the four-momentum transferred to the photon. The vertex function $\Lambda^\mu_{fi}(q)$ is a 3×3 matrix in the neutrino mass eigenstates space that encodes the electromagnetic properties of neutrinos. We are interested in the ultra-relativistic limit where, at low-q^2, it simplifies to,

$$\Lambda^\mu_{fi}(q) = \gamma^\mu\left(Q_{fi} - \frac{q^2}{6}\langle r^2\rangle_{fi}\right) - i\sigma^{\mu\nu}q_\nu\mu_{fi} \quad (2)$$

with $f = i$ for diagonal and $f \neq i$ for transition electromagnetic properties. Note that in theories of massive neutrinos, the transition electromagnetic properties can be generated through mixing, even if the matrices in Eq. (2) are diagonal in the mass basis [35].

In this paper, we conduct a phenomenological study of effective neutrino electromagnetic properties: the millicharge Q, the magnetic moment μ, and the charge radius $\langle r^2\rangle$ at the FPF. Effective here implies the possible inclusion of contributions coming from electric and anapole

moments to the magnetic moment and charge radius [36], respectively. Also, the neutral current interaction we study here has no information on the outgoing neutrino flavor. Therefore, we implicitly assume a sum over all final state neutrino flavors [37,38]. Note that when recasting the results obtained here, e.g., for Majorana neutrinos, they have only transition magnetic moment and millicharge.

The electric neutrality of neutrinos in the SM is guaranteed by charge quantization [39,40]. But in some BSM theories, neutrinos can have a very small electric charge [41] enabling it to couple to the photon. This BSM interaction can be described by an effective term in the Lagrangian $\mathcal{L} \supset Q_\nu(\bar{\nu}\gamma_\mu\nu)A^\mu$.

Neutrino magnetic moments, on the other hand, do arise at one loop level [42,43] for a massive neutrino. The diagonal magnetic moment for a massive Dirac neutrino is given by

$$\mu_\nu \approx \frac{3eG_F}{8\sqrt{2}\pi^2}m_\nu \approx 3 \times 10^{-19}\mu_B\left(\frac{m_\nu}{1\ \mathrm{eV}}\right), \quad (3)$$

where m_ν is the neutrino mass, e is the electric charge, G_F is the Fermi constant and $\mu_B = e/(2m_e)$ is the Bohr magneton. This very small value is beyond the scope of terrestrial and astrophysical probes currently. The values for transition magnetic moments for Majorana neutrinos are even smaller [44]. However, an additional contribution to the magnetic moment of neutrinos could arise from BSM physics [10,12,45]. In an effective field theory approach, this can be parametrized in terms of a higher dimensional operator $\mathcal{L} \supset \mu_\nu(\bar{\nu}\sigma_{\alpha\beta}\nu)F^{\alpha\beta}$ for Dirac neutrinos (for Majorana neutrinos one replaces $\bar{\nu}$ with $\bar{\nu}^c$ for only the left-handed neutrino fields (ν_L) above, and only transition moments are allowed).

Measuring the magnetic moment of neutrinos is important, as it can also in principle shed light on the Dirac vs. Majorana nature of neutrinos. Dirac neutrinos can have diagonal and transition magnetic moments, whereas Majorana neutrinos only have transition magnetic moments. Large transition magnetic moments for Majorana neutrinos could be realized in certain BSM models [46,47], which are not too far from the current experimental limits, but the off-diagonal moments could be hard to measure, as we do not probe the outgoing neutrino flavor.

Neutrinos also have nonzero charge radii in the SM from radiative corrections given by [48,49]

$$\langle r^2_{\nu_\ell}\rangle_{\mathrm{SM}} = \frac{G_F}{4\sqrt{2}\pi^2}\left[3 - 2\log\frac{m^2_\ell}{m^2_W}\right]. \quad (4)$$

where m_ℓ are the lepton masses ($\ell = e, \mu, \tau$) and m_W is the W boson mass. The SM values are then found to be 4.1×10^{-33} cm^2 for ν_e, 2.4×10^{-33} cm^2 for ν_μ and 1.5×10^{-33} cm^2 for ν_τ. These values differ by at most one or two orders of magnitude from current terrestrial bounds,

and hence testing the SM prediction of neutrino charge radius is a compelling challenge.

III. DETECTORS AT THE FPF

An unexpected but powerful source of light and weakly coupled particles can be found at the LHC [50]. In the forward direction, the LHC produces an intense and strongly collimated beam of neutrinos of all three flavors coming mainly from the decays of mesons produced at the interaction point. Currently, there are two experiments taking advantage of this opportunity: FASERν [27,51] and SND@LHC [52,53]. In particular, both experiments are expected to obtain about 20 tau neutrino interactions, which exceeds the number of events recorded by the DONuT [54] and OPERA [55] experiments.

Several improved neutrino detectors are planned for the HL-LHC era. They will be housed in the FPF [28,56] along with an array of other detectors with a wide range of physics potential, to be located in a cavern 620 m downstream from the ATLAS interaction point. Our analysis focuses on two detector technologies at FPF that are sensitive to TeV range neutrino interactions: FLArE, a liquid argon time projection chamber, and FASERν2, an emulsion-based neutrino detector. In the following, we present the detector details relevant to the phenomenological study at hand:

(i) *FLArE*, the Forward Liquid Argon Experiment, is composed of a 10-tonne liquid argon time projection chamber with a fiducial volume of 1 m × 1 m × 7 m [57]. Liquid argon time projection chambers are a proven technology for neutrino physics, having been used at Fermilab's Short-Baseline Neutrino Program [58] and at the future DUNE experiment [59]. They offer the dual advantage of very low energy thresholds of down to 30 MeV and excellent timing resolution, achieved through a light collection system. This will allow one to control possible muon-induced backgrounds by vetoing events in coincidence with a muon track, which is critical to the feasibility of our study. We also include in our study a larger 100-tonne detector, dubbed **FLArE-100**, with a fiducial volume of 1.6 m × 1.6 m × 30 m. This is meant to illustrate how sensitivities would scale with target mass.

(ii) *FASERν2* is an emulsion detector designed as a much larger successor to the approved FASERν detector [60]. In the HL-LHC era, FASERν2 is envisioned as a 10-tonne neutrino detector composed of emulsion layers interleaved with tungsten sheets acting as target material. Emulsion detectors are capable of detecting charged tracks with high spatial resolution. The major drawback of emulsion detectors is a lack of timing information associated with the recorded events. FASERν2 aims to mitigate this by introducing tracking layers between and at the end of the emulsion layers. Timing information

can then be obtained by successfully matching the event in the emulsion and the tracker. This is helpful in the search for a coincident muon track, which can be used to reduce muon-induced backgrounds. We assume that in FASERν2 all muon-induced backgrounds can be eliminated with the help of timing information. The fiducial volume we consider is 0.5 m × 0.5 m × 2 m [61]. Since the charged particle has to pass through a sufficient number of emulsion layers to leave a distinguishable track, a minimum particle momentum of 300 MeV [61] is required. This sets the energy threshold of the detector.

The two processes we study here are neutrino electron elastic scattering and neutral current DIS. The main backgrounds for the former are similar to those studied in Refs. [57,62] and the latter was studied in the context of FASERν in Ref. [63]. Here we briefly summarize the relevant results.

A major source of similar backgrounds for both processes is muon-induced events. Muons passing through the detector can, for example, emit photons through bremsstrahlung or produce high energy neutral hadrons in inelastic scatterings. The photons could then pair convert to e^+e^- and if one of them is missed, it can mimic our electron scattering signal. Neutral hadron scattering, on the other hand, would look similar to the neutral current DIS neutrino interactions. In both cases, the inclusion of timing capabilities in the detectors allows vetoing such backgrounds by associating such events with the accompanying muon. For example, the currently operating FASER detector employs several scintillating veto layers at its front, each of which has a muon detection efficiency of more than 99.99% [64]. In this paper, we assume such muon-induced backgrounds can be reduced to negligible levels.

An irreducible source of backgrounds to both processes is SM contribution to neutral current neutrino scattering. For neutrino electron elastic scattering, we employ the use of kinematic cuts to enhance the signal to background ratio, as described in the next section. This is where a low energy threshold detector like FLArE is advantageous.

Throughout this work, we use the neutrino fluxes presented in Ref. [61] for the HL-LHC era. They were obtained using the event generator `SIBYLL 2.3d` [65–68] implemented via `CRMC` [69] which simulates the primary collision. Ref. [70] introduced a fast neutrino flux simulator that models the propagation and decay of long-lived hadrons within the SM in the forward direction at the LHC. Currently, there exist sizeable uncertainties on the neutrino flux. However, this is expected to be brought under control using the charged current scattering event rate once the detector starts to take data [27].

IV. NEUTRINO EM INTERACTION RATE

The signature we investigate in our study is the excess (or deficit) of neutrino scattering events in the detectors

compared to the expected rate predicted by the SM in the absence of any neutrino EM properties. This can be neutrino electron elastic scattering events or neutral current DIS events.

We first consider the neutrino electron elastic scattering where the SM cross section, in terms of the electron recoil energy E_r, is given by [3,71]

$$\left(\frac{d\sigma_{\nu_\ell e}}{dE_r}\right)_{\rm SM} = \frac{G_F^2 m_e}{2\pi}\left[(g_V^\ell - g_A^\ell)^2\left(1 - \frac{E_r}{E_\nu}\right)^2\right.$$
$$\left. + (g_V^\ell + g_A^\ell)^2 + ((g_A^\ell)^2 - (g_V^\ell)^2)\frac{m_e E_r}{E_\nu^2}\right] \quad (5)$$

with the standard vector and axial vector coupling constants g_A^ℓ and g_A^ℓ given by

$$g_V^\ell = 2\sin^2\theta_W - \frac{1}{2} + \delta_{\ell e}, \qquad g_A^\ell = -\frac{1}{2} + \delta_{\ell e}. \quad (6)$$

Here G_F is the Fermi constant, θ_W is the weak mixing angle, and E_ν is the neutrino energy. For antineutrinos, one must replace g_A^ℓ by $-g_A^\ell$. There is an extra term for the electron neutrino coming from the exchange of the W boson, which is not present for muon and tau neutrinos. In the presence of non-negligible values for the neutrino electromagnetic properties, the event rate and distribution can be sufficiently distorted.

As detailed below, the most significant effect of including these BSM physics is in the event rate, especially at low recoil energies for the magnetic moment and millicharge. This motivates looking at E_r as the main kinematic variable in our study. One could also look at the recoil angle of the electron, as was studied in Ref. [57]. For neutrino electron scatterings at the energies of interest, so E_ν and $E_r \gg m_e$, the recoil angle is correlated with the recoil energy via $\cos\theta_r \approx 1 - m_e/E_r$. Although, this does not help to distinguish different neutrino electron scattering events but provides another handle to remove backgrounds coming from neutrino nuclear scattering events with a single particle recoiling in the final state. Since we will be imposing a strong kinematic cut on the electron recoil energy that suppresses the background sufficiently, we do not include the recoil angle of the electron as an additional observable. We note, however, that the strong correlation between the recoil energy and the recoil angle of the electron can be used to improve energy resolution at small energies.

In some cases, it might be beneficial to also consider nuclear scattering, where one could benefit from higher event rates. As can be seen in Eq. (5), the neutrino electron elastic scattering cross section and hence the event rate is proportional to the target mass m_e. If the new physics signal count decreases or does not increase commensurately, then moving to a heavier target will only degrade the sensitivity. This is the case with neutrino magnetic moment and

millicharge, and hence we stick to electron scattering events for both of them. As we will see below, a charge radius essentially induces a shift in the vector coupling constant, g_V, and hence we can expect higher rates of signal if we use a heavier target. We therefore also consider neutral current neutrino DIS in the charge radius case, which will result in significantly higher signal event rates and hence improve the bounds on $\langle r_{\nu_\ell}^2 \rangle$.

At leading order, the double differential cross section for neutral current neutrino-nucleon DIS is given by [72]

$$\frac{d\sigma(\nu N \to \nu X)}{dxdy}$$
$$= \frac{2G_F^2 m_p E_\nu}{\pi}\frac{m_Z^4}{(Q^2 + m_Z^2)^2}$$
$$\times \sum_{q=u,d,s,c}[g_{q,L}^2[xf_q(x, Q^2) + xf_{\bar{q}}(x, Q^2)(1-y)^2]$$
$$+ g_{q,R}^2[xf_q(x, Q^2)(1-y)^2 + xf_{\bar{q}}(x, Q^2)]] \quad (7)$$

for neutrino scattering and

$$\frac{d\sigma(\bar{\nu} N \to \bar{\nu} X)}{dxdy}$$
$$= \frac{2G_F^2 m_p E_\nu}{\pi}\frac{m_Z^4}{(Q^2 + m_Z^2)^2}$$
$$\times \sum_{q=u,d,s,c}[g_{q,L}^2[xf_q(x, Q^2)(1-y)^2 + xf_{\bar{q}}(x, Q^2)]$$
$$+ g_{q,R}^2[xf_q(x, Q^2) + xf_{\bar{q}}(x, Q^2)(1-y)^2]] \quad (8)$$

for anti-neutrino scattering, where X stands for the final states that are a byproduct of the DIS other than the neutrino. Here m_p is the mass of the target proton, m_Z is the Z boson mass, and $g_L^q, g_R^q = T^3 - Q_q \sin^2\theta_W$ are the left and right-handed neutral current couplings of the quarks with Q_q being the charge of the quarks in units of e, and T^3 being the third component of the quarks's weak isospin. The differential cross section is expressed in terms of the DIS variables x, y and Q^2, where x is the partonic momentum fraction, $y = E_{\rm had}/E_\nu$ is the fraction of neutrino's energy that is transferred to the hadronic system, and $Q^2 = 2m_p E_\nu xy$ is the squared 4-momentum transfer. Here E_ν is the incident neutrino energy, and $E_{\rm had}$ is all the energy contained in the hadronic system. The functions $f_q(x, Q^2)$ are the nucleon parton distribution function. Here we use nCTEQ15 which includes nuclear effects of the target nucleus [73].

A. Neutrino magnetic moment

The presence of a BSM contribution to the neutrino magnetic moment can lead to an excess in the number of electron recoil events, especially at low recoil energies.

The differential cross section with respect to the electron recoil energy for the elastic scattering of a neutrino (or antineutrino) with incoming flavor ℓ and energy E_ν off an electron, in the presence of a magnetic moment, is given by [14,74]

$$\left(\frac{d\sigma_{\nu_\ell e}}{dE_r}\right)_{\mathrm{NMM}} = \left(\frac{d\sigma_{\nu_\ell e}}{dE_r}\right)_{\mathrm{SM}} + \frac{\pi^2}{m_e^2}\left(\frac{1}{E_r}-\frac{1}{E_\nu}\right)\left(\frac{\mu_{\nu_\ell}}{\mu_{\mathrm{B}}}\right)^2, \quad (9)$$

where μ_{ν_ℓ} is the effective neutrino magnetic moment, and μ_B is the Bohr magneton. Note that the two contributions in Eq. (9) add incoherently in the cross section due to the following helicity argument [75]: in the ultra-relativistic limit, the SM weak interaction conserves the neutrino helicity while the helicity flips in the neutrino magnetic moment interaction. Hence, one is always guaranteed an excess of events in this case.

The two contributions in the cross section exhibit quite different dependencies in the electron recoil energy E_r, as illustrated in Fig. 1 top left panel for an incoming neutrino beam with 1 TeV energy. The signal cross section associated with the neutrino magnetic moment exceeds the SM background in the range,

$$E_r \lesssim 10 \text{ GeV} \times \left(\frac{\mu_{\nu_\ell}}{10^{-8}\mu_{\mathrm{B}}}\right)^2. \quad (10)$$

This leads to an increase in the elastic neutrino-electron events above the SM predicted value at low values of E_r. This can be seen as arising from the $1/E_r$ term in the BSM cross section expression. The lines for ν_e and $\nu_{\mu,\tau}$ differ due to the additional diagram from the W boson exchange, which is only present for ν_e.

Given the neutrino flux at the FPF, the electron recoil energy spectrum at FLArE and FASERν2 detectors can be calculated. Figure 1 top right panel shows the total expected event rate for a benchmark value of $\mu_{\nu_\ell} = 10^{-8}\mu_B$ for all three flavors at FLArE, as well as the SM event rate. The three flavors of neutrinos have different fluxes at FPF, resulting in distinct predictions for the event spectrum. The excess events in the low recoil energy bins serve as an experimental signature to look for neutrino magnetic moment.

B. Neutrino millicharge

The FPF is an ideal environment to search for millicharged particles in the dark sector [76,77] and can also be used to probe neutrino millicharge. The inclusion of a nonzero electric charge for the neutrino changes the neutrino-electron elastic scattering cross section as [3,35,78]

$$\left(\frac{d\sigma_{\nu_\ell e}}{dE_r}\right)_{\mathrm{NMC}} = \left(\frac{d\sigma_{\nu_\ell e}}{dE_r}\right)_{\mathrm{SM}} + \left(\frac{d\sigma_{\nu_\ell e}}{dE_r}\right)_{\mathrm{Int}} + \left(\frac{d\sigma_{\nu_\ell e}}{dE_r}\right)_{\mathrm{Quad}}. \quad (11)$$

The first term is the above SM expression as before. The interference term is,

$$\left(\frac{d\sigma_{\nu_\ell e}}{dE_r}\right)_{\mathrm{Int}} = \frac{\sqrt{8\pi}G_F\alpha}{E_\nu^2 E_r}\left(\frac{Q_{\nu_\ell}}{e}\right)[g_V^\ell(2E_\nu^2+E_r^2$$
$$- E_r(2E_\nu+E_r)) + g_A^\ell(E_r(2E_\nu-E_r))] \quad (12)$$

with g_V^ℓ, g_A^ℓ defined as before, and the quadratic term is given by

$$\left(\frac{d\sigma_{\nu_\ell e}}{dE_r}\right)_{\mathrm{Quad}} = 4(\pi\alpha)^2\left(\frac{Q_{\nu_\ell}}{e}\right)^2\left[\frac{2E_\nu^2+E_r^2-2E_\nu E_r}{m_e E_r^2 E_\nu^2}\right], \quad (13)$$

where Q_{ν_ℓ} is the electric charge of the neutrino in units of e. For anti-neutrino, we replace g_A with $-g_A$ similar to the SM case. The presence of the interference term $\sim Q_{\nu_\ell}$ means we are now sensitive to the sign of the neutrino millicharge and depending on the value of Q_{ν_ℓ} we can expect an increase or decrease in the number of events. However, it turns out that, for the values of the millicharge that can be probed at the FPF, the quadratic term always dominates, therefore, an excess of events is expected. For a benchmark value of $Q_{\nu_\ell} = 10^{-7}e$ we see an even steeper increase in cross section at lower recoil energies than for the magnetic moment, as the quadratic term grows proportionally to $1/E_r^2$. This is shown in Fig. 1 middle left panel, while the middle right panel shows the event spectrum at FLArE.

Alternatively, neutrino millicharge can also be probed at FORMOSA [76], a proposed experiment located within the FPF to search for millicharged particles. If neutrino possesses a millicharge, then it will ionize the material and deposit energy as it passes through the detector, resulting in a scintillation signature. FORMOSA is a dedicated detector to detect low-charge scintillation signals consisting of an array of plastic scintillators with multiple layers, sensitive to low-energy deposits down to one single photoelectron. The mean ionization energy loss for a millicharged neutrino travelling through the plastic material can be estimated by Bethe-Bloch formula [79] that goes as $\langle dE/dx \rangle \sim (Q_\nu/e)^2 \times 5$ MeV/cm, and is quite insensitive to the neutrino energy and mass. The average number of photoelectrons produced within a scintillator bar N_{PE} is proportional to the ionization energy deposition, the bar length, and the scintillation light yield. To suppress the background noise in the photomultiplier tubes attached to the scintillation bars that collect the produced photoelectrons, the low-energy scintillation signal candidates are required to have multiple coincidences of hits. To detect a millicharged neutrino, at least one photoelectron in each layer of the scintillator must be observed. The detection probability $P = (1 - \exp(-N_{\mathrm{PE}}))^n$ follows the Poisson distribution, where n is the number of layers.
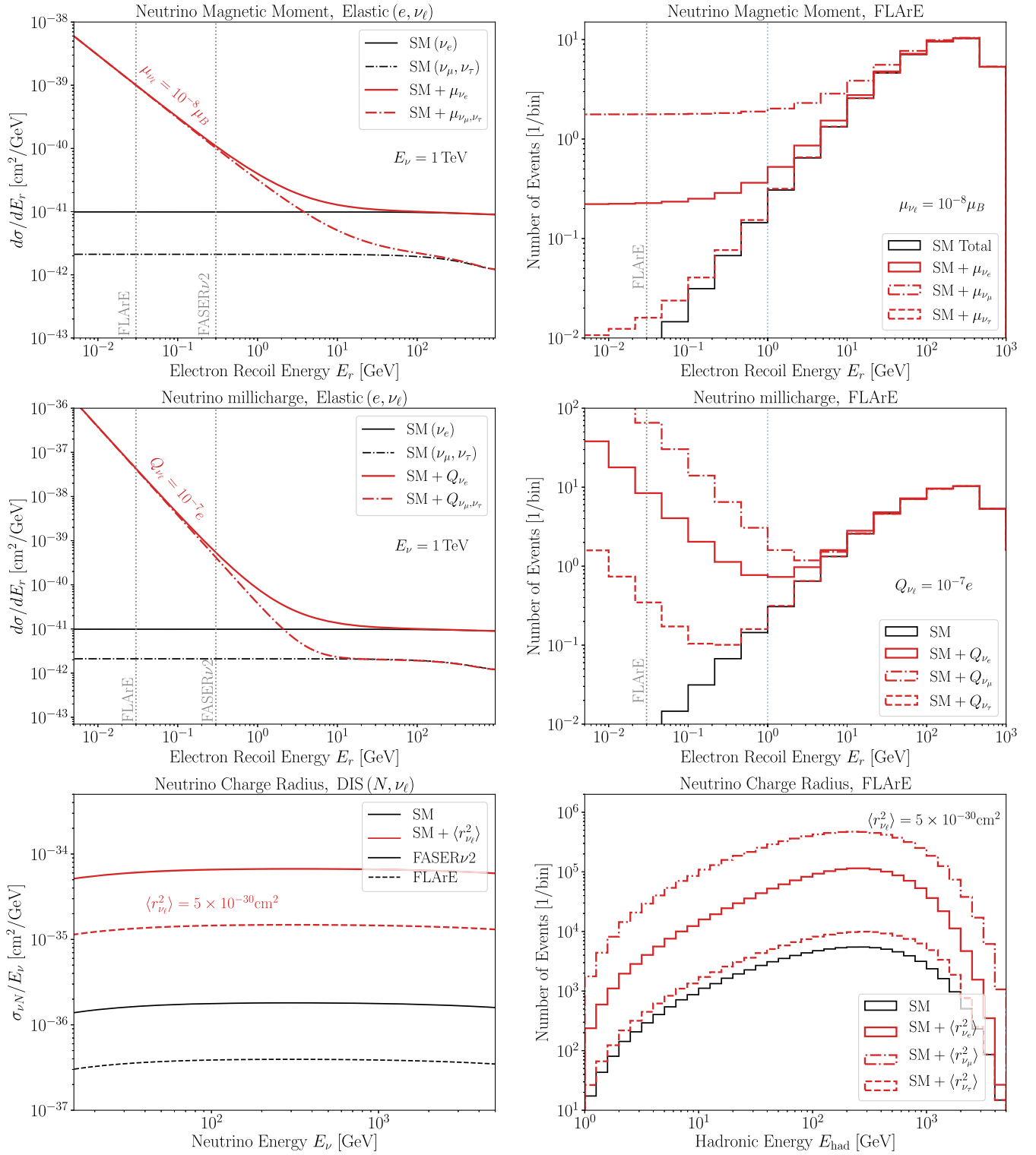
FIG. 1. Top and middle left: differential cross-section of neutrino elastic scattering on the electron as a function of electron recoil energy, corresponding to the incoming neutrino energy of 1 TeV. Top and middle right: the expected number of events at FLArE, considering the estimated neutrino flux at the FPF in the HL-LHC phase. The magnetic moment and millicharge electromagnetic contributions (red) exceed the SM background (black) at lower recoil energies. The FLArE and FASERν2 detector recoil energy thresholds of 30 and 300 MeV, as well as the 1 GeV upper cutoff, are indicated by vertical dotted lines. Bottom left: cross section of neutrino-nucleus deep-inelastic scattering in FASERν2 (solid) and FLArE (dashed) as a function of neutrino energy, within the SM (black) and in the presence of the charge radius. Bottom right: expected event rate at FLArE as a function of the energy of the hadronic system.

C. Neutrino charge radius

From Eq. (2), one sees that a nonzero value of charge radius amounts to a shift in the vector term of the neutrino vertex function. Within the SM, only diagonal charge radii are allowed, as generation lepton numbers are conserved. However, some BSM scenarios also allow for off-diagonal charge radii [80–82]. If we only consider diagonal elements in the flavor basis, it was shown in Ref. [43] that this amounts to a modification of the vector coupling constant in Eq. (6) as,

$$g_V^\ell \to g_V^\ell + \frac{2}{3} m_W^2 \langle r_{\nu_\ell}^2 \rangle \sin^2\theta_W. \qquad (14)$$

This introduces additional linear and quadratic terms in $\langle r_{\nu_\ell}^2 \rangle$ to the cross section in Eq. (5). Therefore, similar to the neutrino millicharge case, we are sensitive to the sign of $\langle r_{\nu_\ell}^2 \rangle$. Also, note that the antineutrino charge radius contribution comes with a negative relative sign to the above shift [3]. For quarks, this shift is modified by the quark-to-electron electric charge ratio as,

$$g_V^q \to g_V^q - \frac{2}{3} Q_q m_W^2 \langle r_{\nu_\ell}^2 \rangle \sin^2\theta_W \qquad (15)$$

which modifies the left and right-handed neutral current couplings of the quarks $g_{L/R}^q = (g_V^q \pm g_A^q)/2$ in Eqs. (7) and (8).

In the bottom left panel of Fig. 1, we show the DIS cross section rates for a neutrino scattering off the argon nucleus in the FLArE detector and tungsten nucleus in the FASERν2 detector as a function of the incoming neutrino energy, E_ν. FASERν2 with a target atom with a higher atomic number has more nucleons for the neutrino to scatter off and hence has a higher cross section value. In the presence of a nonzero charge radius, the cross section

enhancement is almost uniform across the incoming neutrino energy range. In the bottom right panel, we show the event spectrum as a function of E_{had} at FLArE for a benchmark value of $\langle r_{\nu_e}^2 \rangle = 5 \times 10^{-30}$ cm^2. At the neutrino energies available at FPF and the values of $\langle r_{\nu_\ell}^2 \rangle$ we are sensitive to, it is the quadratic term that is dominant, and we observe an excess in events across the spectrum.

V. SENSITIVITY FOR NEUTRINO EM PROPERTIES

We are now ready to turn to our analysis. As described in the previous section, both the neutrino magnetic moment and neutrino millicharge would manifest themselves through an enhanced rate of neutrino-electron scattering events with low electron recoil energy. To isolate this effect, we select events within the energy range $E_{\mathrm{thr}} < E_r < 1$ GeV. Here we assume a lower energy threshold of $E_{\mathrm{thr}} = 30$ MeV for FLArE and 300 MeV for FASERν2. According to Refs. [57,77], after applying these kinematic cuts, we expect less than $\mathcal{O}(1)$ neutrino-electron scattering events in the SM. Considering statistical uncertainties only, we do a log-likelihood ratio analysis where the number of expected events follow a Poisson distribution, allowing us to set limits on neutrino magnetic moment and millicharge. Systematic uncertainties are expected to be under control since the neutrino-electron cross section is well understood and the neutrino fluxes can be constrained by the same experiment through a measurement of the event rate of neutrino charged current scattering [83]. Notably, for the considered events with small electron recoil energies, the SM event rate is small, and therefore neutrino flux uncertainties are less relevant than for neutrino charge radius measurements.

We present projected sensitivity on neutrino magnetic moment and millicharge in the upper part of Table 1.

TABLE I. Projected 90% C.L. sensitivity on neutrino electromagnetic properties (μ_{ν_ℓ}, Q_{ν_ℓ}, $\langle r_{\nu_\ell}^2 \rangle$) from FASER$\nu$2, FLArE, FLArE-100 detectors for all three flavors, assuming 3 ab^{-1} of integrated luminosity at HL-LHC. For completeness, we also show the charge radius bounds from electron scattering in the last row, which, as expected, are much weaker compared to those from nuclear scattering.

Neutrino EM property		FASERν2	FLArE	FLArE-100
μ_{ν_ℓ} [$10^{-8}\mu_B$]	ν_e	1.78	1.35	0.73
	ν_μ	0.67	0.48	0.25
	ν_τ	10.7	6.59	3.08
Q_{ν_ℓ} [$10^{-8}e$]	ν_e	[−13.1, 8.92]	[−4.03, 3.21]	[−2.21, 1.52]
	ν_μ	[−3.92, 4.12]	[−0.96, 1.27]	[−0.24, 0.30]
	ν_τ	[−64.9, 65.1]	[−17.9, 17.9]	[−8.33, 8.36]
$\langle r_{\nu_\ell}^2 \rangle$ [10^{-32} cm^2]	ν_e	[−3.57, 4.46]	[−3.47, 4.29]	[−1.43, 1.55]
	ν_μ	[−0.65, 0.67]	[−0.62, 0.64]	[−0.25, 0.25]
Nuclear scattering	ν_τ	[−58.9, 96.1]	[−41.3, 78.4]	[−17.3, 54.8]
$\langle r_{\nu_\ell}^2 \rangle$ [10^{-31} cm^2]	ν_e	[−1.11, 0.85]	[−1.62, 1.10]	[−0.54, 0.47]
	ν_μ	[−0.86, 1.70]	[−1.03, 1.79]	[−0.56, 1.29]
Electron scattering	ν_τ	[−16.4, 16.6]	[−14.5, 14.8]	[−7.53, 8.04]

The upper bounds are given for different flavors at FASERν2, FLArE, and FLArE-100, considering an integrated luminosity of 3 ab^{-1} at HL-LHC. Note that the bounds are slightly sensitive to the sign of the neutrino millicharge due to the presence of the interference terms.

Unlike the other two neutrino properties, the effect of a neutrino charge radius is not confined to a specific energy region. Instead, we search for an increased neutrino scattering event rate across the whole energy spectrum. For this, we consider both the electron scattering and nuclear scattering channel, where the latter will turn out to be more sensitive due to the significantly larger overall event rate. As this nuclear scattering channel is essentially a precision measurement of the total neutral current scattering rate, it is subject to systematic uncertainties, which we discuss below.

One major source of systematic uncertainties is associated with the neutrino flux. While the uncertainties on the LHC neutrino flux predictions are currently large [70,84–87], a measurement of the charged current event rate will constrain the fluxes once the experiment starts taking data. In our analysis, we take this into account by considering the statistical uncertainty expected in the measurement of charged current events as a proxy for the uncertainty on the flux estimates.

Another source of uncertainty is associated with the modelling of the neutrino-nucleus interaction cross section. This includes, for example, parton distribution functions, quark mass effects, higher order radiative corrections, nuclear shadowing and anti-shadowing effects, the modelling of parton shower and hadronization inside the target nucleus, as well as final state interactions. A recent prediction using the NNSFν neutrino structure functions introduced in Ref. [88] quotes a 2.5–3% uncertainty on the cross section for the energy range 100 GeV $< E_\nu <$ few TeV, which is relevant to this study. We will use this result as a conservative estimate. Future measurements like at the FPF [89] and EIC [90,91] will reduce these uncertainties and bring to a 1% level. Though these uncertainties are quoted for charge current interactions, we expect them to be similar for neutral current interactions as the underlying PDFs are the same. We illustrate the effect of this by showing results for 3% and 1% uncertainty. We note that cross section modelling uncertainties quoted in the weak mixing angle analysis performed by NuTeV [4] were around 0.3%, and therefore even smaller than the values assumed here, indicating that even a 1% uncertainty is not unrealistic. Hence, we also show the results for 0.3% uncertainty as an optimistic case and with 0% uncertainty to illustrate what the best case scenario could be.

Finally, there could be uncertainties arising from the experimental setup, for example, related to energy reconstruction, detection efficiency, particle identification, and event classification. In particular, very soft leptons from CC interactions can be missed and be mistaken for NC events. Since the detector designs are still under development, the details on the detector performance are not yet available. However, this also leaves room to consider the signatures under discussion in this study as a benchmark for detector design and optimize them accordingly. In the following, we assume that detector-related uncertainties can be sufficiently reduced to be smaller than the statistical and cross section uncertainties of the measurement.

Unlike neutrino magnetic moment and millicharge measurements, here we look at the entire energy spectrum ($E_r > E_{\mathrm{thr}}$), and hence we expect higher event rates. So we employ a χ^2 analysis to set bounds on neutrino charge radius that can be probed at these forward detectors. We consider statistical uncertainty and also systematic uncertainties coming from neutrino flux and neutrino-nucleus cross section. As mentioned above, uncertainty on the neutrino flux estimate is included by considering the statistical uncertainty in the CC events as a proxy. For systematic uncertainty on the neutrino-nucleus cross section, we include a pull parameter with an uncertainty of 3%, 1%, and 0.3%. The projected sensitivity on neutrino charge radius, considering only statistical uncertainties and systematic uncertainty coming from the neutrino flux, are presented in the lower part of Table I. As expected, the bounds obtained from the electron scattering signature are much weaker compared to those from nuclear scattering. In Table II, we show the results for neutrino charge radius from nuclear scattering only, including various values for cross section uncertainty. We see how going from 0% to 3% weakens the bound by roughly a factor of few for FLArE.

The obtained sensitives (without cross section uncertainties) to the neutrino EM properties are also presented in Fig. 2, alongside existing constraints and relevant benchmark scenarios. Here we show only the positive bounds, as the negative values are very similar in absolute value. A recent projection on the sensitivity for electron and muon neutrinos at DUNE, as obtained in Ref. [78], is also shown for comparison.

The left panel shows the results for the neutrino magnetic moment. Shown as dark gray shaded regions are current constraints obtained by purely laboratory experiments using reactor and accelerator neutrinos from GEMMA [16], TEXONO [17], LAMPF [20], LSND [18] and DONUT [19]. The light gray shaded region corresponds to measurements using solar neutrinos at Borexino [22], XENONnT [6,24,92] and LZ [24,25]. We can see that FLArE will be able to provide the leading sensitivity to tau neutrino magnetic moment obtained using a pure laboratory measurement and constrain $\mu_{\nu_\tau} \lesssim 7 \times 10^{-8}\mu_B$. This is due to the large flux of tau neutrino at the LHC location compared with other laboratory neutrino sources.

Throughout the years, a variety of new physics models predicting large neutrino magnetic moments have been proposed [10,11,45]. Such scenarios have been revisited recently in Refs. [13,14]. The authors conclude that models of Dirac neutrinos with large diagonal neutrino magnetic

TABLE II.   Same as Table 1 but only for neutrino charge radius from nuclear scattering. Now we include an uncertainty of 3%, 1%, 0.3%, and 0% on the neutrino-nucleus cross section. Results for 0% are the same as those shown in Table 1.

Neutrino charge radius		FASERν2	FLArE	FLArE-100
$\langle r^2_{\nu_e}\rangle$ [10^{-32} cm^2]	3%	[−13.5, 50.1]	[−13.8, 51.1]	[−13.5, 51.4]
	1%	[−6.05, 9.16]	[−6.09, 9.11]	[−5.35, 7.33]
	0.3%	[−3.86, 4.92]	[−4.31, 5.60]	[−3.04, 3.58]
	0%	[−3.57, 4.46]	[−3.47, 4.29]	[−1.43, 1.55]
$\langle r^2_{\nu_\mu}\rangle$ [10^{-32} cm^2]	3%	[−2.93, 3.03]	[−2.93, 3.04]	[−2.90, 3.01]
	1%	[−1.15, 1.18]	[−1.14, 1.17]	[−1.00, 1.01]
	0.3%	[−0.70, 0.72]	[−0.78, 0.80]	[−0.54, 0.55]
	0%	[−0.65, 0.67]	[−0.62, 0.64]	[−0.25, 0.25]
$\langle r^2_{\nu_\tau}\rangle$ [10^{-32} cm^2]	3%	[−146.4, 183.6]	[−109.9, 146.9]	[−91.1, 128.6]
	1%	[−84.0, 121.2]	[−61.3, 98.4]	[−46.3, 83.8]
	0.3%	[−62.1, 99.3]	[−48.1, 85.2]	[−30.7, 68.1]
	0%	[−58.9, 96.1]	[−41.3, 78.4]	[−17.3, 54.8]

moments do not seem possible anymore unless one is willing to accept it to be fine-tuned. An example of such a scenario was found in Ref. [12] in a scan over the MSSM parameter space, where a muon magnetic neutrino magnetic moment as large as $10^{-9}\mu_B$ was found. In contrast, for Majorana neutrinos, large transition moments can be realized, for example using a $SU(2)_H$ horizontal symmetry [46] or a BFZ model [47]. We illustrate those scenarios as the green region in Fig. 2. In addition, large neutrino magnetic moments have been used to explain the existence of black holes in the mass-gap region that have been detected in the gravitational wave event GW190521 [8]. The corresponding region is marked in blue.

We present the results for neutrino millicharge in the middle panel of Fig. 2. As before, the dark-shaded regions show purely laboratory constraints from DONUT [19,41], LSND [18,41], Dresden-II [93], CONUS [94], TEXONO [95,96], and GEMMA [96,97]. Upper limits on neutrino millicharge have been also obtained using solar neutrinos by XMASS [98], XENONnT [6,24,92] and LZ [24,25] as shown by the light gray shaded regions. Not included in this figure are additional constraints from astrophysical considerations, since they are subject to additional underlying assumptions and uncertainties compared to pure laboratory constraints. In particular, the neutrino millicharge can have an impact on astrophysical phenomena
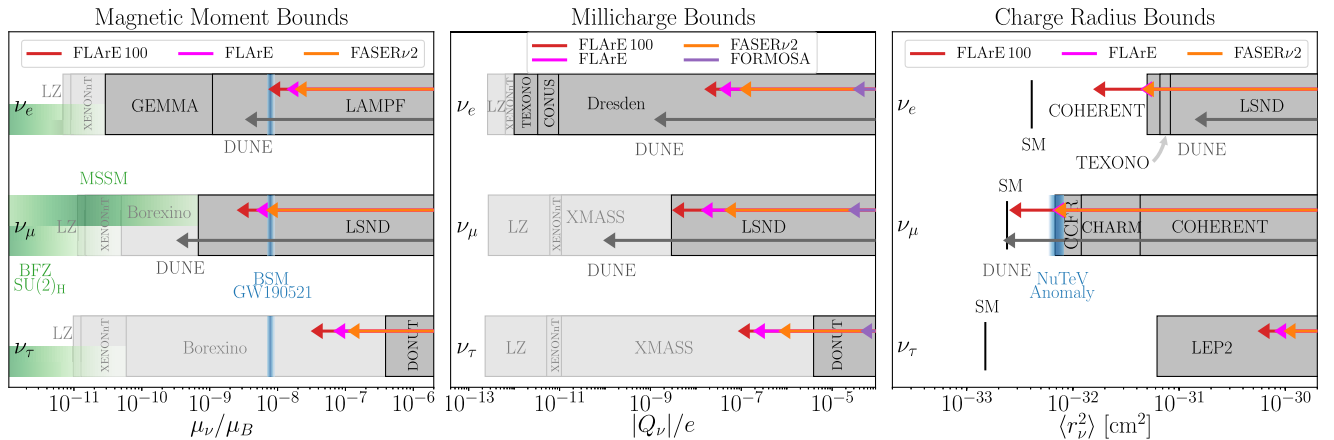

FIG. 2.   Comparison of experimental bounds on neutrino electromagnetic properties: effective magnetic moment (left), millicharge (middle), and charge radius (right). The projected sensitivity of FASERν2 (orange), FLArE (magenta), and FLArE-100 (red) shown alongside existing accelerator and reactor constraints (dark gray shaded), direct detection limits from solar neutrino flux (light gray shaded) and projections from other proposed searches (gray arrow). The FASERν2, and FLArE(-100) results in this plot consider only statistical and flux uncertainties. The blue-shaded regions correspond to the magnetic moment values that explain the NuTeV anomaly, and gravitational waves signal from black hole mergers. The contribution of BSM benchmark models to large magnetic moments is presented in green. FLArE can set the world's leading limits on neutrino magnetic moment and millicharge for tau neutrino coming from terrestrially produced neutrinos, and set the world's leading limit for electron neutrino charge radius. The limits on muon neutrino charge radius for FLArE come within a factor of a few from the SM prediction.

such as red giant or solar cooling [99], the rotation of magnetized neutron stars [100], and the arrival time of SN 1987A supernova neutrinos [101], resulting in approximate upper limits on the effective charge of electron neutrino in the range $|Q_{\nu_e}| \lesssim 10^{-14} - 10^{-19}$. Even stronger constraints than astrophysical arguments on the electron neutrino milli-charge can be obtained from electric charge conservation in neutron beta decay, along with the experimental bounds on the neutron charge and the non-neutrality of matter giving $|Q_{\nu_e}| \lesssim 10^{-21}e$ [99]. We find that FLArE is potentially capable of providing the most stringent limit on the effective electric charge of tau neutrino from terrestrially produced neutrinos, with an upper limit of $|Q_{\nu_\tau}| \lesssim 10^{-7}e$.

Following the study of millicharged particles using the scintillator-based experiment [76,102], we can expect to bound the neutrino millicharge at FORMOSA to $|Q_{\nu_e}| \lesssim 2.8 \times 10^{-5}e$, $|Q_{\nu_\mu}| \lesssim 2.2 \times 10^{-5}e$, and $|Q_{\nu_\tau}| \lesssim 4.1 \times 10^{-5}e$ with 90% C.L., corresponding to a scintillator detector with quadruple coincidence. These upper bounds on neutrino millicharge, which are weaker than FLArE results, are presented in the middle panel of Fig. 2. These projected sensitivities are almost independent of the neutrino flux, as the sensitivity is limited by the fact that below $Q_\nu \sim 5 \times 10^{-4}e$, the probability of photoelectron production drops significantly. The analysis of FORMOSA with 4 layers is considered almost background free. To demonstrate the sensitivity reach, we also assume zero background for a detector with triple coincidence and find the 90% C.L. upper bounds $|Q_{\nu_e}| \lesssim 0.8 \times 10^{-5}e$, $|Q_{\nu_\mu}| \lesssim 0.5 \times 10^{-5}e$, and $|Q_{\nu_\tau}| \lesssim 1.3 \times 10^{-5}e$. This background-free assumption can in principle be achieved, for example, by using better photomultiplier tubes (PMTs) that have less background noise.

The right panel shows the results for the neutrino charge radius. The dark gray shaded regions are current constraints obtained by purely laboratory experiments using reactor and accelerator neutrinos from COHERENT [93,103], CHARM-II [104], LSND [18], CCFR [105,106], LEP2 [106], TEXONO [107]. FLArE can set the world's leading limit for electron neutrino and set highly competitive limits for muon neutrino where it comes within a factor of a few from the SM prediction. The deviation of the weak mixing angle from the SM observed by the NuTeV Collaboration [4] could also be interpreted as a measurement of the muon neutrino charge radius $\langle r_{\nu_\mu}^2 \rangle = 4.20 \times 10^{-33}$ within 1σ error [106]. The 1σ preferred region to explain the NuTeV anomaly is shown by the blue target region.[1] For comparison, DUNE is expected to constrain $|\langle r_{\nu_\mu}^2 \rangle| < 2 \times 10^{-33}$ cm^2 and $|\langle r_{\nu_e}^2 \rangle| < 1 \times 10^{-31}$ cm^2, which is an order of magnitude

weaker than the FLArE bound for the electron neutrino. The DUNE projection considered the electron scattering signature, which suffers from lower event rates. A measurement using nuclear scattering at DUNE does not seem promising due to the large nuclear uncertainties in the cross section for GeV energy neutrinos.

VI. MEASUREMENT OF THE WEAK MIXING ANGLE AND THE NUTEV ANOMALY

The measurement of neutrino interactions at the energies accessible at the FPF provides an opportunity to measure precisely the electroweak parameters. The weak mixing angle, $\sin^2\theta_W$, is one key parameter that parametrizes several measurable observables in the electroweak sector of the SM. The value of $\sin^2\theta_W$ gets radiative corrections and depends on the renormalization prescription [111], where $\overline{\text{MS}}$ (modified minimal subtraction) scheme is conventionally employed. One of the best measurements of the weak mixing angle comes from Z-pole observables [79,112] (Tevatron, LEP1, SLC, LHC) with an average value of $\sin^2\theta_W(m_Z)_{\overline{\text{MS}}} = 0.23125(16)$, comparable to the SM value of $\sin^2\theta_W(m_Z)_{\overline{\text{MS}}} = 0.23122(4)$ [79]. At relatively low energy scales, several experimental measurements of weak mixing angle exist (for a review, see Ref. [113]) including the electron-deep inelastic scattering [114] (eDIS), neutrino-nucleus scattering [4] (NuTeV), atomic parity violation [115–118] (APV on cesium), Moller scattering [119] (SLAC E158), elastic electron-proton scattering [120] (Q_{weak}), and coherent elastic neu-trino-nucleus scattering at COHERENT [121] and Dresden-II [122]. The precise measurement of the weak mixing angle at different energy scales provides a direct probe of new physics beyond the SM [113,123,124]. In particular, it will allow one to test the NuTeV anomaly [4]. Using neutrino scattering, the collaboration measured a value of $\sin^2\theta_W$ that was 3σ above the SM prediction at a scale of ~ 4 GeV. A measurement at FPF will shed more light on the running of the weak mixing angle at a similar energy scale. Any change in the weak mixing angle from the SM value, $\sin^2\theta_W \to \sin^2\theta_W + \Delta\sin^2\theta_W$, will result in a shift in the vector coupling constant,

$$g_V^q \to g_V^q - 2Q_q \Delta\sin^2\theta_W. \quad (16)$$

The phenomenological consequences of this shift are therefore very similar to the study of neutrino charge radius presented in the previous section. We perform a similar analysis to obtain the FLArE expected sensitivity to the weak mixing angle and constrain $\Delta\sin^2\theta_W < 0.0077$ at 68% C.L. The estimate for sensitivity to $\sin^2\theta_W$ in the $\overline{\text{MS}}$ scheme at the scale $\mu \sim Q \sim 10$ GeV, which is the typical momentum transfer for a TeV scale energy neutrino at FLArE, is shown in Fig. 3, along with the existing constraints and the running of the coupling predicted by the SM [79,111,125]. Results are shown for different values

---

[1]While there exist many possible ways to explain this anomaly with new physics [108], a reassessment of the NuTeV results [109,110] with more careful considerations suggest that this result is in agreement with the SM prediction.
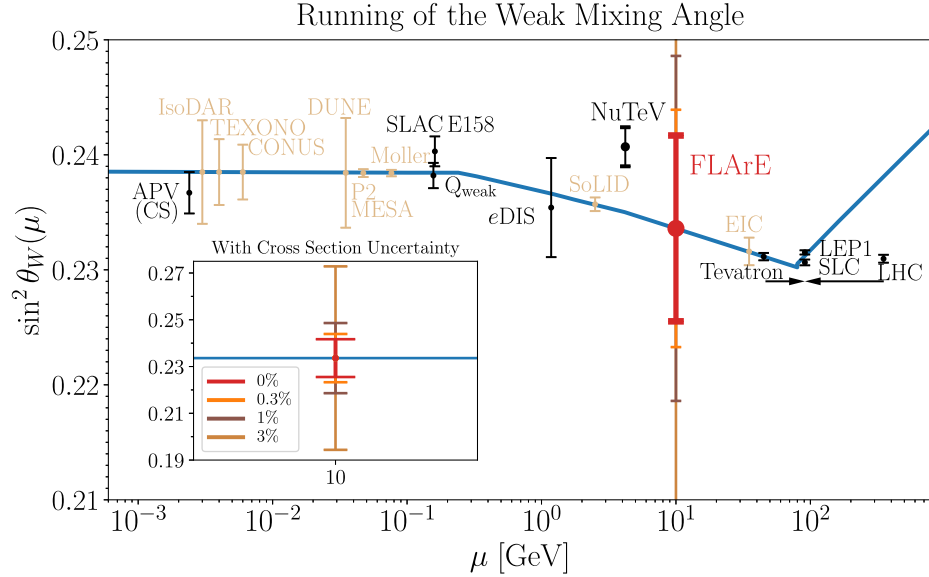
FIG. 3.   Scale dependence of the weak mixing angle in the $\overline{\text{MS}}$ scheme, $\sin^2 \theta_W(\mu)$, shown with the existing measurements (black), the expected sensitivity of FLArE at FPF (red), and other future experiments (beige). The blue line corresponds to the SM prediction for the running of $\sin^2 \theta_W$ with scale μ. For clarity, the Tevatron and LHC points are shifted horizontally on either side. Inset: we also show the sensitivity only at FLArE including a 3%, 1%, 0.3% and 0% systematic uncertainty on the neutrino-nucleus cross section.

of cross section uncertainty. For comparison, we also show the projected sensitivities to the weak mixing angle from future experiments including DUNE [126], EIC [127], Moller at JLAB [119,128], MESA-P2 [129], SoLID at JLAB [130], IsoDAR at Yemilab [131], and reactors [132–135] (TEXONO, CONUS).

A precise measurement of the weak mixing angle requires good control over various systematic uncertainties. These are analogous to the measurement of the neutrino charge radius through nuclear scattering, and we refer the reader to the previous section for a more detailed discussion. As before, we have considered statistical uncertainties as well as uncertainties associated with flux normalization as constrained by charged current measurements, and neutrino-nucleus cross section in our sensitivity estimate. It is worth noting that the measurement of the weak mixing angle provides a well-motivated benchmark for detector performance requirements that should be considered during detector design.

VII. CONCLUSION

The immense flux of neutrinos in the forward region of the LHC provides an excellent opportunity for neutrino physics. This neutrino beam is a powerful source of the most energetic human-made neutrinos for all three flavors. The proposed neutrino detectors at the FPF, FASERν2 and FLArE, can use this neutrino beam to set stringent constraints on neutrino electromagnetic properties and measure the weak mixing angle to percent level precision.

In this paper, we have presented a detailed phenomenological study on the potential of the FPF experiments to probe the neutrino electromagnetic properties: magnetic moment, millicharge and charge radius. All these scenarios result in an excess of neutral current events that can be observed at these detectors. We first look at neutrino-electron elastic scattering, where in the presence of neutrino magnetic moment and millicharge the excess events are at low electron recoil energies. Focusing on this kinematic region and taking advantage of the huge tau neutrino flux, FPF can set the strongest limits on neutrino magnetic moment and millicharge for tau neutrinos coming from terrestrially produced neutrinos. For neutrino charge radius, better constraints are obtained by looking at the neutral current neutrino DIS process, where the heavier target results in an increased event rate over neutrino-electron elastic scattering. By looking for excess events across the entire spectrum, FPF can set the world's leading limits on the neutrino charge radius for electron neutrinos and, for muon neutrinos, FPF can come within a factor of a few from the SM prediction. We have summarized our results in Table 1 and Fig. 2.

An important test of the SM is the measurement of electroweak parameters at different energy scales. FPF has the potential to measure the weak mixing angle with a precision of about 3% at an energy scale of $\mu \sim 10$ GeV. In Fig. 3, we show the scale dependence of the weak mixing angle along with the FPF measurement, which considers both statistical and flux uncertainties. This is an important test of the SM, especially in light of the NuTeV anomaly. The ability to measure the weak mixing angle with high precision sets an important benchmark for the design of the FPF neutrino detectors.

[1] R. E. Shrock, Electromagnetic properties and decays of Dirac and Majorana neutrinos in a general class of gauge theories, Nucl. Phys. **B206,** 359 (1982).

[2] J.-M. Frère, J. Heeck, and S. Mollet, Triangle inequalities for Majorana-neutrino magnetic moments, Phys. Rev. D **92,** 053002 (2015).

[3] C. Giunti and A. Studenikin, Neutrino electromagnetic interactions: A window to new physics, Rev. Mod. Phys. **87,** 531 (2015).

[4] G. P. Zeller *et al.* (NuTeV Collaboration), A precise determination of electroweak parameters in neutrino nucleon scattering, Phys. Rev. Lett. **88,** 091802 (2002); **90,** 239902(E) (2003).

[5] E. Aprile *et al.* (XENON Collaboration), Excess electronic recoil events in XENON1T, Phys. Rev. D **102,** 072004 (2020).

[6] E. Aprile *et al.* (XENON Collaboration), Search for new physics in electronic recoil data from XENONnT, Phys. Rev. Lett. **129,** 161805 (2022).

[7] D. Croon, S. D. McDermott, and J. Sakstein, Missing in axion: Where are XENON1T's big black holes?, Phys. Dark Universe **32,** 100801 (2021).

[8] J. Sakstein, D. Croon, S. D. McDermott, M. C. Straight, and E. J. Baxter, Beyond the Standard Model explanations of GW190521, Phys. Rev. Lett. **125,** 261105 (2020).

[9] M. B. Voloshin, On compatibility of small mass with large magnetic moment of neutrino, Sov. J. Nucl. Phys. **48,** 512 (1988).

[10] R. Barbieri and R. N. Mohapatra, A neutrino with a large magnetic moment and a naturally small mass, Phys. Lett. B **218,** 225 (1989).

[11] S. Rajpoot, Dirac neutrino magnetic moments in the left-right symmetric model, Phys. Lett. B **237,** 77 (1990).

[12] A. Aboubrahim, T. Ibrahim, A. Itani, and P. Nath, Large neutrino magnetic dipole moments in MSSM extensions, Phys. Rev. D **89,** 055009 (2014).

[13] M. Lindner, B. Radovčić, and J. Welter, Revisiting large neutrino magnetic moments, J. High Energy Phys. 07 (2017) 139.

[14] K. S. Babu, S. Jana, and M. Lindner, Large neutrino magnetic moments in the light of recent experiments, J. High Energy Phys. 10 (2020) 040.

[15] K. S. Babu, S. Jana, M. Lindner, and V. P. K, Muon $g − 2$ anomaly and neutrino magnetic moments, J. High Energy Phys. 10 (2021) 240.

[16] A. G. Beda, V. B. Brudanin, V. G. Egorov, D. V. Medvedev, V. S. Pogosov, M. V. Shirchenko, and A. S. Starostin, The results of search for the neutrino magnetic moment in GEMMA experiment, Adv. High Energy Phys. **2012,** 350150 (2012).

[17] H. T. Wong *et al.* (TEXONO Collaboration), A search of neutrino magnetic moments with a high-purity germanium detector at the Kuo-Sheng nuclear power station, Phys. Rev. D **75,** 012001 (2007).

[18] L. B. Auerbach *et al.* (LSND Collaboration), Measurement of electron—neutrino—electron elastic scattering, Phys. Rev. D **63,** 112001 (2001).

[19] R. Schwienhorst *et al.* (DONUT Collaboration), A new upper limit for the tau—neutrino magnetic moment, Phys. Lett. B **513,** 23 (2001).

[20] R. C. Allen *et al.*, Study of electron-neutrino electron elastic scattering at LAMPF, Phys. Rev. D **47,** 11 (1993).

[21] C. Arpesella *et al.* (Borexino Collaboration), Direct measurement of the Be-7 solar neutrino flux with 192 days of Borexino data, Phys. Rev. Lett. **101,** 091302 (2008).

[22] M. Agostini *et al.* (Borexino Collaboration), Limiting neutrino magnetic moments with Borexino Phase-II solar neutrino data, Phys. Rev. D **96,** 091103 (2017).

[23] P. Coloma, M. C. Gonzalez-Garcia, M. Maltoni, J. a. P. Pinheiro, and S. Urrea, Constraining new physics with Borexino Phase-II spectral data, J. High Energy Phys. 07 (2022) 138.

[24] S. K. A., A. Majumdar, D. K. Papoulias, H. Prajapati, and R. Srivastava, Implications of first LZ and XENONnT results: A comparative study of neutrino properties and light mediators, Phys. Lett. B **839,** 137742 (2023).

[25] J. Aalbers *et al.* (LZ Collaboration), First dark matter search results from the LUX-ZEPLIN (LZ) experiment, Phys. Rev. Lett. **131,** 041002 (2023).

[26] D. Aristizabal Sierra, O. G. Miranda, D. K. Papoulias, and G. S. Garcia, Neutrino magnetic and electric dipole moments: From measurements to parameter space, Phys. Rev. D **105,** 035027 (2022).

[27] H. Abreu *et al.* (FASER Collaboration), Detecting and studying high-energy collider neutrinos with FASER at the LHC, Eur. Phys. J. C **80**, 61 (2020).

[28] L. A. Anchordoqui *et al.*, The forward physics facility: Sites, experiments, and physics potential, Phys. Rep. **968**, 1 (2022).

[29] G. Magill, R. Plestid, M. Pospelov, and Y.-D. Tsai, Dipole portal to heavy neutral leptons, Phys. Rev. D **98**, 115015 (2018).

[30] I. M. Shoemaker, Y.-D. Tsai, and J. Wyenberg, Active-to-sterile neutrino dipole portal and the XENON1T excess, Phys. Rev. D **104**, 115026 (2021).

[31] A. Ismail, S. Jana, and R. M. Abraham, Neutrino up-scattering via the dipole portal at forward LHC detectors, Phys. Rev. D **105**, 055008 (2022).

[32] K. Jodłowski and S. Trojanowski, Neutrino beam-dump experiment with FASER at the LHC, J. High Energy Phys. 05 (2021) 191.

[33] B. Kayser, Majorana neutrinos and their electromagnetic properties, Phys. Rev. D **26**, 1662 (1982).

[34] J. F. Nieves, Electromagnetic properties of Majorana neutrinos, Phys. Rev. D **26**, 3152 (1982).

[35] K. A. Kouzakov and A. I. Studenikin, Electromagnetic properties of massive neutrinos in low-energy elastic neutrino-electron scattering, Phys. Rev. D **95**, 055013 (2017); **96**, 099904(E) (2017).

[36] C. Giunti, J. Gruszko, B. Jones, L. Kaufman, D. Parno, and A. Pocar, Report of the topical group on neutrino properties for snowmass 2021, arXiv:2209.03340.

[37] W. Grimus and T. Schwetz, Elastic neutrino electron scattering of solar neutrinos and potential effects of magnetic and electric dipole moments, Nucl. Phys. **B587**, 45 (2000).

[38] J. F. Beacom and P. Vogel, Neutrino magnetic moments, flavor mixing, and the Super-Kamiokande solar data, Phys. Rev. Lett. **83**, 5222 (1999).

[39] C. Q. Geng and R. E. Marshak, Uniqueness of quark and lepton representations in the Standard Model from the anomalies viewpoint, Phys. Rev. D **39**, 693 (1989).

[40] K. S. Babu and R. N. Mohapatra, Quantization of electric charge from anomaly constraints and a Majorana neutrino, Phys. Rev. D **41**, 271 (1990).

[41] A. Das, D. Ghosh, C. Giunti, and A. Thalapillil, Neutrino charge constraints from scattering to the weak gravity conjecture to neutron stars, Phys. Rev. D **102**, 115009 (2020).

[42] K. Fujikawa and R. Shrock, The magnetic moment of a massive neutrino and neutrino spin rotation, Phys. Rev. Lett. **45**, 963 (1980).

[43] P. Vogel and J. Engel, Neutrino electromagnetic form-factors, Phys. Rev. D **39**, 3378 (1989).

[44] P. B. Pal and L. Wolfenstein, Radiative decays of massive neutrinos, Phys. Rev. D **25**, 766 (1982).

[45] R. N. Mohapatra, S.-P. Ng, and H.-b. Yu, Reactor searches for neutrino magnetic moment as a probe of extra dimensions, Phys. Rev. D **70**, 057301 (2004).

[46] K. S. Babu and R. N. Mohapatra, Model for large transition magnetic moment of the ν_e, Phys. Rev. Lett. **63**, 228 (1989).

[47] S. M. Barr, E. M. Freire, and A. Zee, A mechanism for large neutrino magnetic moments, Phys. Rev. Lett. **65**, 2626 (1990).

[48] J. Bernabeu, J. Papavassiliou, and J. Vidal, The neutrino charge radius is a physical observable, Nucl. Phys. **B680**, 450 (2004).

[49] J. Bernabeu, L. G. Cabral-Rosetti, J. Papavassiliou, and J. Vidal, On the charge radius of the neutrino, Phys. Rev. D **62**, 113012 (2000).

[50] J. L. Feng, I. Galon, F. Kling, and S. Trojanowski, Forward search experiment at the LHC, Phys. Rev. D **97**, 035001 (2018).

[51] H. Abreu *et al.* (FASER Collaboration), Technical proposal: FASERnu, arXiv:2001.03073.

[52] C. Ahdida *et al.*, SND@LHC—scattering and neutrino detector at the LHC, CERN, Geneva, Technical Reports No. CERN-LHCC-2021-003, No. LHCC-P-016, 2021, https://cds.cern.ch/record/2750060.

[53] C. Ahdida *et al.* (SHiP Collaboration), SND@LHC, arXiv:2002.08722.

[54] K. Kodama *et al.* (DONuT Collaboration), Final tau-neutrino results from the DONuT experiment, Phys. Rev. D **78**, 052002 (2008).

[55] N. Agafonova *et al.* (OPERA Collaboration), Final results of the OPERA experiment on ν_τ appearance in the CNGS neutrino beam, Phys. Rev. Lett. **120**, 211801 (2018).

[56] J. L. Feng *et al.*, The forward physics facility at the high-luminosity LHC, J. Phys. G **50**, 030501 (2023).

[57] B. Batell, J. L. Feng, and S. Trojanowski, Detecting dark matter with far-forward emulsion and liquid argon detectors at the LHC, Phys. Rev. D **103**, 075023 (2021).

[58] M. Antonello *et al.* (MicroBooNE, LAr1-ND, and ICARUS-WA104 Collaborations), A proposal for a three detector short-baseline neutrino oscillation program in the Fermilab booster neutrino beam, arXiv:1503.01520.

[59] B. Abi *et al.* (DUNE Collaboration), Deep underground neutrino experiment (DUNE), Far detector technical design report, Volume II: DUNE physics, arXiv:2002.03005.

[60] FASER Collaboration, FASERν2: A forward neutrino experiment at the HL LHC, https://www.snowmass21 .org/docs/files/summaries/NF/SNOWMASS21-NF10_NF6-EF6_EF9-IF0_FASERnu2-006.pdf.

[61] B. Batell, J. L. Feng, A. Ismail, F. Kling, R. M. Abraham, and S. Trojanowski, Discovering dark matter at the LHC through its nuclear scattering in far-forward emulsion and liquid argon detectors, Phys. Rev. D **104**, 035036 (2021).

[62] B. Batell, J. L. Feng, M. Fieg, A. Ismail, F. Kling, R. M. Abraham, and S. Trojanowski, Hadrophilic dark sectors at the forward physics facility, Phys. Rev. D **105**, 075001 (2022).

[63] A. Ismail, R. Mammen Abraham, and F. Kling, Neutral current neutrino interactions at FASERν, Phys. Rev. D **103**, 056014 (2021).

[64] H. Abreu *et al.* (FASER Collaboration), The FASER detector, J. Instrum. **19**, P05066 (2024).

[65] E.-J. Ahn, R. Engel, T. K. Gaisser, P. Lipari, and T. Stanev, Cosmic ray interaction event generator SIBYLL 2.1, Phys. Rev. D **80**, 094003 (2009).

[66] F. Riehn, R. Engel, A. Fedynitch, T. K. Gaisser, and T. Stanev, A new version of the event generator Sibyll, *Proc. Sci.*, ICRC2015 (2016) 558 [arXiv:1510.00568].

[67] F. Riehn, H. P. Dembinski, R. Engel, A. Fedynitch, T. K. Gaisser, and T. Stanev, The hadronic interaction model SIBYLL 2.3c and Feynman scaling, *Proc. Sci.*, ICRC2017 (2018) 301 [arXiv:1709.07227].

[68] F. Riehn, R. Engel, A. Fedynitch, T. K. Gaisser, and T. Stanev, Hadronic interaction model Sibyll 2.3d and extensive air showers, Phys. Rev. D **102,** 063002 (2020).

[69] R. Ulrich, T. Pierog, and C. Baus, Cosmic ray Monte Carlo package, CRMC, 10.5281/zenodo.5270381 (2021).

[70] F. Kling and L. J. Nevay, Forward neutrino fluxes at the LHC, Phys. Rev. D **104,** 113008 (2021).

[71] J. A. Formaggio and G. P. Zeller, From eV to EeV: Neutrino cross sections across energy scales, Rev. Mod. Phys. **84,** 1307 (2012).

[72] K. S. McFarland, Neutrino interactions, in *Procedings of the 61st Scottish Universities Summer School in Physics: Neutrinos in Particle Physics, Astrophysics and Cosmology (SUSSP61)* (2008), pp. 65–90; arXiv:0804.3899.

[73] K. Kovarik *et al.*, nCTEQ15—Global analysis of nuclear parton distributions with uncertainties in the CTEQ framework, Phys. Rev. D **93,** 085037 (2016).

[74] A. de Gouvea and J. Jenkins, What can we learn from neutrino electron scattering?, Phys. Rev. D **74,** 033004 (2006).

[75] W. Grimus and P. Stockinger, Effects of neutrino oscillations and neutrino magnetic moments on elastic neutrino—electron scattering, Phys. Rev. D **57,** 1762 (1998).

[76] S. Foroughi-Abari, F. Kling, and Y.-D. Tsai, Looking forward to millicharged dark sectors at the LHC, Phys. Rev. D **104,** 035014 (2021).

[77] F. Kling, J.-L. Kuo, S. Trojanowski, and Y.-D. Tsai, Flare up dark sectors with EM form factors at the LHC forward physics facility, Nucl. Phys. **B987,** 116103 (2023).

[78] V. Mathur, I. M. Shoemaker, and Z. Tabrizi, Using DUNE to shed light on the electromagnetic properties of neutrinos, J. High Energy Phys. 10 (2022) 041.

[79] R. L. Workman *et al.* (Particle Data Group), Review of particle physics, Prog. Theor. Exp. Phys. **2022,** 083C01 (2022).

[80] M. Cadeddu, F. Dordei, C. Giunti, Y. F. Li, E. Picciau, and Y. Y. Zhang, Physics results from the first COHERENT observation of coherent elastic neutrino-nucleus scattering in argon and their combination with cesium-iodide data, Phys. Rev. D **102,** 015030 (2020).

[81] J. Bernstein and T. D. Lee, Electromagnetic form-factor of the neutrinos, Phys. Rev. Lett. **11,** 512 (1963).

[82] A. Grau and J. A. Grifols, Neutrino charge radius and substructure, Phys. Lett. **166B,** 233 (1986).

[83] F. Kling, T. Mäkelä, and S. Trojanowski, Investigating the fluxes and physics potential of LHC neutrino experiments, Phys. Rev. D **108,** 095020 (2023).

[84] W. Bai, M. Diwan, M. V. Garzelli, Y. S. Jeong, and M. H. Reno, Far-forward neutrinos at the large hadron collider, J. High Energy Phys. 06 (2020) 032.

[85] Y. S. Jeong, W. Bai, M. Diwan, M. V. Garzelli, F. K. Kumar, and M. H. Reno, Neutrinos from charm: Forward production at the LHC and in the atmosphere, *Proc. Sci.*, ICRC2021 (2021) 1218 [arXiv:2107.01178].

[86] R. Maciula and A. Szczurek, Far-forward production of charm mesons and neutrinos at forward physics facilities at the LHC and the intrinsic charm in the proton, Phys. Rev. D **107,** 034002 (2023).

[87] R. Mammen Abraham *et al.* (FASER Collaboration), Neutrino rate predictions for FASER, Phys. Rev. D **110,** 012009 (2024).

[88] A. Candido, A. Garcia, G. Magni, T. Rabemananjara, J. Rojo, and R. Stegeman, Neutrino structure functions from GeV to EeV energies, J. High Energy Phys. 05 (2023) 149.

[89] J. M. Cruz-Martinez, M. Fieg, T. Giani, P. Krack, T. Mäkelä, T. R. Rabemananjara, and J. Rojo, The LHC as a neutrino-ion collider, Eur. Phys. J. C **84,** 369 (2024).

[90] R. A. Khalek, J. J. Ethier, E. R. Nocera, and J. Rojo, Self-consistent determination of proton and nuclear PDFs at the electron ion collider, Phys. Rev. D **103,** 096005 (2021).

[91] R. Abdul Khalek, J. J. Ethier, and J. Rojo (NNPDF Collaboration), Nuclear parton distributions from lepton-nucleus scattering and the impact of an electron-ion collider, Eur. Phys. J. C **79,** 471 (2019).

[92] A. N. Khan, Light new physics and neutrino electromagnetic interactions in XENONnT, Phys. Lett. B **837,** 137650 (2023).

[93] M. Atzori Corona, M. Cadeddu, N. Cargioli, F. Dordei, C. Giunti, Y. F. Li, C. A. Ternes, and Y. Y. Zhang, Impact of the Dresden-II and COHERENT neutrino scattering data on neutrino electromagnetic properties and electroweak physics, J. High Energy Phys. 09 (2022) 164.

[94] H. Bonet *et al.* (CONUS Collaboration), First upper limits on neutrino electromagnetic properties from the CONUS experiment, Eur. Phys. J. C **82,** 813 (2022).

[95] S. N. Gninenko, N. V. Krasnikov, and A. Rubbia, Search for millicharged particles in reactor neutrino experiments: A probe of the PVLAS anomaly, Phys. Rev. D **75,** 075014 (2007).

[96] J.-W. Chen, H.-C. Chi, H.-B. Li, C. P. Liu, L. Singh, H. T. Wong, C.-L. Wu, and C.-P. Wu, Constraints on millicharged neutrinos via analysis of data from atomic ionizations with germanium detectors at sub-keV sensitivities, Phys. Rev. D **90,** 011301 (2014).

[97] A. Studenikin, New bounds on neutrino electric millicharge from limits on neutrino magnetic moment, Europhys. Lett. **107,** 21001 (2014); **107,** 39901(E) (2014).

[98] K. Abe *et al.* (XMASS Collaboration), Search for exotic neutrino-electron interactions using solar neutrinos in XMASS-I, Phys. Lett. B **809,** 135741 (2020).

[99] G. G. Raffelt, Limits on neutrino electromagnetic properties: An update, Phys. Rep. **320,** 319 (1999).

[100] A. I. Studenikin and I. Tokarev, Millicharged neutrino with anomalous magnetic moment in rotating magnetized matter, Nucl. Phys. **B884,** 396 (2014).

[101] G. Barbiellini and G. Cocconi, Electric charge of the neutrinos from SN1987A, Nature (London) **329,** 21 (1987).

[102] K. J. Kelly and Y.-D. Tsai, Proton fixed-target scintillation experiment to search for millicharged dark matter, Phys. Rev. D **100,** 015043 (2019).

[103] A. N. Khan, Neutrino millicharge and other electromagnetic interactions with COHERENT-2021 data, Nucl. Phys. **B986,** 116064 (2023).

[104] P. Vilain *et al.* (CHARM-II Collaboration), Experimental study of electromagnetic properties of the muon-neutrino in neutrino—electron scattering, Phys. Lett. B **345**, 115 (1995).

[105] K. S. McFarland *et al.* (CCFR, E744, and E770 Collaborations), A precision measurement of electroweak parameters in neutrino—nucleon scattering, Eur. Phys. J. C **1**, 509 (1998).

[106] M. Hirsch, E. Nardi, and D. Restrepo, Bounds on the tau and muon neutrino vector and axial vector charge radius, Phys. Rev. D **67**, 033005 (2003).

[107] M. Deniz *et al.* (TEXONO Collaboration), Measurement of Nu(e)-bar -electron scattering cross-section with a CsI (Tl) scintillating crystal array at the Kuo-Sheng nuclear power reactor, Phys. Rev. D **81**, 072001 (2010).

[108] S. Davidson, S. Forte, P. Gambino, N. Rius, and A. Strumia, Old and new physics interpretations of the NuTeV anomaly, J. High Energy Phys. 02 (2002) 037.

[109] S. J. Brodsky, I. Schmidt, and J.-J. Yang, Nuclear antishadowing in neutrino deep inelastic scattering, Phys. Rev. D **70**, 116003 (2004).

[110] W. Bentz, I. C. Cloet, J. T. Londergan, and A. W. Thomas, Reassessment of the NuTeV determination of the weak mixing angle, Phys. Lett. B **693**, 462 (2010).

[111] J. Erler and M. J. Ramsey-Musolf, The weak mixing angle at low energies, Phys. Rev. D **72**, 073003 (2005).

[112] ALEPH, CDF, D0, DELPHI, L3, OPAL, SLD, LEP Electroweak Working Group, Tevatron Electroweak Working Group, SLD Electroweak, Heavy Flavour Groups Collaborations, Precision electroweak measurements and constraints on the standard model, arXiv:1012.2367.

[113] K. S. Kumar, S. Mantry, W. J. Marciano, and P. A. Souder, Low energy measurements of the weak mixing angle, Annu. Rev. Nucl. Part. Sci. **63**, 237 (2013).

[114] D. Wang *et al.* (PVDIS Collaboration), Measurement of parity violation in electron–quark scattering, Nature (London) **506**, 67 (2014).

[115] C. S. Wood, S. C. Bennett, D. Cho, B. P. Masterson, J. L. Roberts, C. E. Tanner, and C. E. Wieman, Measurement of parity nonconservation and an anapole moment in cesium, Science **275**, 1759 (1997).

[116] J. Guena, M. Lintz, and M. A. Bouchiat, Measurement of the parity violating $6S - 7S$ transition amplitude in cesium achieved within 2×10^{-13} atomic-unit accuracy by stimulated-emission detection, Phys. Rev. A **71**, 042108 (2005).

[117] V. A. Dzuba, J. C. Berengut, V. V. Flambaum, and B. Roberts, Revisiting parity non-conservation in cesium, Phys. Rev. Lett. **109**, 203003 (2012).

[118] M. S. Safronova, D. Budker, D. DeMille, D. F. J. Kimball, A. Derevianko, and C. W. Clark, Search for new physics with atoms and molecules, Rev. Mod. Phys. **90**, 025008 (2018).

[119] P. L. Anthony *et al.* (SLAC E158 Collaboration), Precision measurement of the weak mixing angle in Moller scattering, Phys. Rev. Lett. **95**, 081601 (2005).

[120] D. Androić *et al.* (Qweak Collaboration), Precision measurement of the weak charge of the proton, Nature (London) **557**, 207 (2018).

[121] D. Akimov *et al.* (COHERENT Collaboration), Measurement of the coherent elastic neutrino-nucleus scattering cross section on CsI by COHERENT, Phys. Rev. Lett. **129**, 081801 (2022).

[122] A. Majumdar, D. K. Papoulias, R. Srivastava, and J. W. F. Valle, Physics implications of recent Dresden-II reactor data, Phys. Rev. D **106**, 093010 (2022).

[123] H. Davoudiasl, H.-S. Lee, and W. J. Marciano, Muon anomaly and dark parity violation, Phys. Rev. Lett. **109**, 031802 (2012).

[124] H. Davoudiasl, H.-S. Lee, and W. J. Marciano, Low Q^2 weak mixing angle measurements and rare Higgs decays, Phys. Rev. D **92**, 055005 (2015).

[125] J. Erler and R. Ferro-Hernández, Weak mixing angle in the Thomson limit, J. High Energy Phys. 03 (2018) 196.

[126] A. de Gouvea, P. A. N. Machado, Y. F. Perez-Gonzalez, and Z. Tabrizi, Measuring the weak mixing angle in the DUNE near detector complex, Phys. Rev. Lett. **125**, 051803 (2020).

[127] R. Boughezal, A. Emmert, T. Kutz, S. Mantry, M. Nycz, F. Petriello, K. Şimşek, D. Wiegand, and X. Zheng, Neutral-current electroweak physics and SMEFT studies at the EIC, Phys. Rev. D **106**, 016006 (2022).

[128] J. Mammei (MOLLER Collaboration), The MOLLER experiment, Nuovo Cimento Soc. Ital. Fis. **035N04C**, 203 (2012).

[129] N. Berger *et al.*, Measuring the weak mixing angle with the P2 experiment at MESA, J. Univ. Sci. Tech. China **46**, 481 (2016).

[130] P. A. Souder (H1 and ZEUS Collaborations), Parity-violating PVDIS with SoLID, AIP Conf. Proc. **1441**, 123 (2012).

[131] J. Alonso *et al.*, Neutrino physics opportunities with the IsoDAR source at Yemilab, Phys. Rev. D **105**, 052009 (2022).

[132] T. S. Kosmas, O. G. Miranda, D. K. Papoulias, M. Tortola, and J. W. F. Valle, Sensitivities to neutrino electromagnetic properties at the TEXONO experiment, Phys. Lett. B **750**, 459 (2015).

[133] B. C. Canas, E. A. Garces, O. G. Miranda, M. Tortola, and J. W. F. Valle, The weak mixing angle from low energy neutrino measurements: A global update, Phys. Lett. B **761**, 450 (2016).

[134] B. C. Cañas, E. A. Garcés, O. G. Miranda, and A. Parada, Future perspectives for a weak mixing angle measurement in coherent elastic neutrino nucleus scattering experiments, Phys. Lett. B **784**, 159 (2018).

[135] M. Lindner, W. Rodejohann, and X.-J. Xu, Coherent neutrino-nucleus scattering and new neutrino interactions, J. High Energy Phys. 03 (2017) 097.

[136] F. Kling and S. Trojanowski, Forward experiment sensitivity estimator for the LHC and future hadron colliders, Phys. Rev. D **104**, 035012 (2021).

[137] A. Buckley, J. Ferrando, S. Lloyd, K. Nordström, B. Page, M. Rüfenacht, M. Schönherr, and G. Watt, LHAPDF6: Parton density access in the LHC precision era, Eur. Phys. J. C **75**, 132 (2015).